PHYSICAL REVIEW A VOLUME 24, NUMBER 2 AUGUST 1981

Far-infrared superradiance in methyl fluoride

A. T. Rosenberger*
Department of Physics, University of Illinois, Urbana, Illinois 61801

T. A. DeTemple
Department of Electrical Engineering and Coordinated Science Laboratory, University of Illinois, Urbana, Illinois 61801
(Received 3 November 1980)

Superradiance has been observed in the far infrared on a pure-rotational transition in optically pumped methyl fluoride. Observed behavior included single pulses, shot-to-shot fluctuation, dependence on the pump pulse length, preferential polarization, and longitudinally asymmetric emission (the onset of swept-gain superradiance). A numerical solution of the Maxwell-Bloch equations including degeneracy, Doppler broadening, and population and polarization source terms, and taking into account all the transitions which might possibly contribute, produces results which agree well with the observations. To do this, only a single free parameter is used; this is a factor of about 10 multiplying the expected initial tipping angle (which is of the order of $N^{-1/2}$).

I. INTRODUCTION

Superradiance, as first discussed by Dicke,[1] is the coherent spontaneous emission of an ensemble of atoms or molecules. The emitting atoms act cooperatively as a result of being coupled by their common radiation field and the superradiant emission is characteristically a pulse of peak intensity proportional to the square of N, the number of cooperating atoms. The emitted pulse is delayed from the time of simultaneous excitation by an interval inversely proportional to N, has a duration inversely proportional to N, and has a spectral width proportional to N.

In the 25 years since Dicke's work appeared, many papers on the theory of superradiance have been published.[2-31] These have greatly extended and refined the treatment of cooperative spontaneous emission in a system of initially inverted two-level atoms. The theories fall into two main groups, fully quantum[4-21] and semiclassical[21-26] theories. The latter treat the atoms quantum mechanically but the fields classically, using the coupled Maxwell-Bloch equations[32] and requiring as initial condition a slight tipping angle of the Bloch vector, i.e., incomplete inversion. The former employ quantized fields and naturally include spontaneous emission so that no "initial tipping angle" is necessary; the emission process may begin from a state of full inversion. If this fully inverted initial state is produced incoherently, coherence will develop spontaneously as the emission proceeds; this special case of cooperative spontaneous emission is called superfluorescence.[19] Our use of the term "superradiance" rather than "superfluorescence" is intentional; we do not want to imply that the initial excitation is totally incoherent.

In contrast to the extensive theoretical literature, relatively few superradiance experiments have been reported.[33-45] The first experiment, in optically pumped HF gas,[33] showed, rather than a single pulse, several of successively decreasing amplitude ("ringing"). This was interpreted as an effect of propagation.[24] Later experiments in optically pumped Cs vapor[37] showed that single pulses could be obtained under conditions, unlike those in previous experiments, where Doppler broadening was insignificant; however, some of the Cs pulses also exhibited a form of ringing. This is thought to be a transverse radiation effect.[20] The comparison of theory and experimental results has been, on the whole, rather inconclusive; some of the reasons for this include the questions of the proper form of the semiclassical initial condition, the detailed dependence of the delay on N, the shot-to-shot fluctuation, and the pulse shapes. In part, this inconclusiveness results from rather large experimental uncertainties in N, a difficult quantity to measure.

In this paper, we cannot claim to present the final solution to any of these problems. We do believe, however, that the excitation process, level degeneracy, emission polarization, and line broadening must all be considered in comparing our experimental results with the semiclassical theory. When they are, quite good agreement results for a wide range of experimental conditions from the judicious choice of a single free parameter. When any one of them is not considered, poorer agreement results; agreement with the mean-field theory is also poor and will not be discussed here.

Our experiment[38] involves the observation of superradiant emission at a wavelength of 496 μm from methyl fluoride (CH_3F) gas optically pumped by a CO_2 transversely excited atmosphere (TEA) laser. We observe no ringing, probably because homogeneous (collision) broadening is a signifi-

cant factor in our experiment. Our data range from the regime of collision broadening to that of Doppler broadening, and from the conditions of Dicke superradiance (equivalent emission from the two ends of the cylindrical sample) to those of swept-gain superradiance [27-31,42] (dominance of emission in the direction of propagation of the pump—forward emission). Finally, because of the partial coherence and finite duration of the pump pulse, the CH_3F (neglecting degeneracy and parallel transitions) should be treated as a three-level system, prompting our use of the more general term superradiance.

The experiment will be discussed in detail in the next section. Section III is devoted to the semiclassical theory: the Maxwell-Bloch equations and their numerical solution and a comparison of their predictions with our data. The main results of this paper are summarized in Sec. IV.

II. EXPERIMENT

A. Properties of CH_3F

Methyl fluoride was used as the experimental system in order to follow up earlier results which had suggested the occurrence of superradiant emission in optically pumped CH_3F.[46] The present study was made possible by development of new techniques of optical pumping and detection, in particular, the plasma-shutter method of pump pulse truncation and a fast, sensitive far-infrared (FIR) detector. In this system, it was also hoped that it would be possible to study directly the influence of homogeneous broadening on the superradiant emission process. In addition, the spectroscopy of CH_3F is well known, so that there should be little ambiguity in the numerical modeling.

Several of the physical parameters of CH_3F are listed in Table I. The $P(20)$ laser line of CO_2 at 9.55 μm is absorbed by several ν_3-mode vibrational-rotational transitions in CH_3F, as shown in Fig. 1. This partial energy-level diagram for CH_3F shows three absorption-emission possibilities; others, for values of K as large as seven have been observed,[53] although in most cases, that for $K=2$ dominates. Of the pure rotational emissions shown, only the ones at 496 μm have been observed by us; the other two wavelengths, if present, are too weak to be detected. Of the collisional processes shown in Fig. 1, only the rotational relaxation is fast enough to be of concern during the ten to few hundred nanoseconds between excitation and emission. Because the molecular vibration-rotation constants of the ν_3 mode are well known,[54] the pump laser detunings and FIR emission frequencies may be calculated. The fractional population in each of the initial $J=12$ states of interest may also be calculated, and these are given in Table II

TABLE I. Physical parameters of methyl fluoride.

Doppler width $\Delta\nu_D$ at 9.55 μm	67 MHz
$T_2^* \left[\equiv\left(\frac{\ln 2}{\pi}\right)^{1/2}\frac{1}{\Delta\nu_D}\right]$ at 496 μm	1.29 MHz
$T_2^* \left[\equiv\left(\frac{\ln 2}{\pi}\right)^{1/2}\frac{1}{\Delta\nu_D}\right]$ at 9.55 μm	7.01 nsec
$T_2^* \left[\equiv\left(\frac{\ln 2}{\pi}\right)^{1/2}\frac{1}{\Delta\nu_D}\right]$ at 496 μm	364 nsec
Homogeneous linewidth $\Delta\nu_H$	40 MHz/Torr[a]
$T_2 \left(\equiv\frac{1}{\pi\Delta\nu_H}\right)$	7.96 nsec Torr
Rotational relaxation rate Γ_R $(=1/T_2)$	1.26×10^8 sec^{-1} Torr^{-1}
K-changing collision rate Γ_K	1.2×10^7 sec^{-1} Torr^{-1} [b]
Vibration-vibration relaxation rate Γ_V	1.2×10^5 sec^{-1} Torr^{-1} [c]
Vibration-translation relaxation rate Γ_{VT}	600 sec^{-1} Torr^{-1} [c]
Permanent dipole moment μ (ground state)	1.8585 D[d]
($v=1$, ν_3 mode)	1.9054 D[e]
Transition dipole moment μ_{ir}	0.205 D[f]

[a] Estimated from theoretical (Ref. 47) and experimental (Refs. 48 and 49) results.
[b] Assumed to be gas kinetic; see Ref. 50 and references therein.
[c] Reference 50.
[d] Reference 51.
[e] Reference 52.
[f] Calculated from the results of Ref. 49.

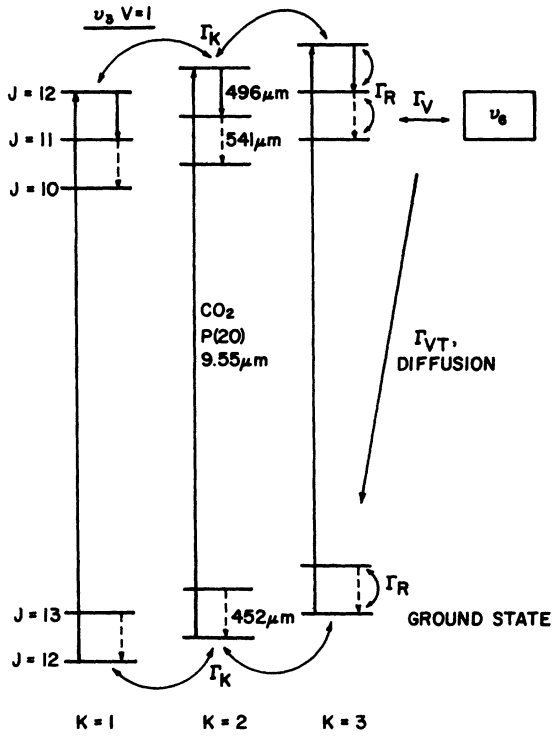

FIG. 1. Partial energy level diagram of the ν_3 mode of CH_3F showing radiative and collisional processes.

with the detunings and FIR spontaneous emission lifetimes for the values of K relevant to our experiment.

B. Apparatus

The experimental setup is shown in Fig. 2. The infrared (ir) 9.55 μm pulse from a CO_2 TEA laser is truncated by a plasma shutter, its polarization

TABLE II. Absorption and emission parameters. Here, f is the fraction of the population found in the lower $J=12$ state at 300 K. The quantity Δ_a is the absorption detuning: absorption transition frequency minus pump laser frequency. Δ_e is the emission frequency detuning relative to $K=2$, and λ is the emission wavelength. The spontaneous lifetime T_{sp} is the real lifetime, including emission into all polarizations.

K	f (%)	Δ_a (MHz)	Δ_e (MHz)	λ (μm)	T_{sp} (sec)
1	0.689	−42	39	496.07	224.9
2	0.649	44	0	496.10	229.8
3	1.17	192	−66	496.16	238.4

is rotated, it is passed through a cell containing methyl fluoride, and the transmitted pulse is detected and recorded. The subsequent FIR emission propagates in both directions, emission one way being absorbed to eliminate feedback, and emission the other way being detected and recorded.

The CO_2 laser is grating tunable and consists of a transversely excited atmospheric pressure (TEA) section in series with a low-pressure cw longitudinal discharge cell for single-mode operation.[55] Its smooth output pulse is about 150 nsec long and has an energy of 250 mJ in an output spot size of 0.5 cm^2. The entire CO_2 laser is mounted in an Invar frame for structural and thermal stability and the TEA discharge and its associated electronics are shielded for electrical noise suppression.

The plasma shutter[56] consists of two confocal germanium lenses between which clean nitrogen gas flows. Near the focus, a small surface-dielectric spark gap, driven by a fast Marx bank

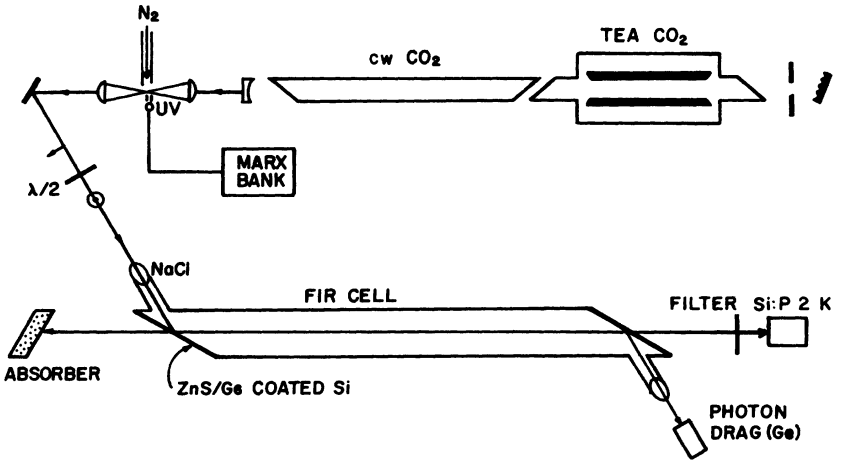

FIG. 2. Experimental arrangement showing CO_2 laser, plasma shutter, methyl fluoride cell, and detector.

pulser[57] which is triggered by the TEA laser discharge, seeds the focal volume with ionizing ultraviolet radiation. When the laser pulse intensity reaches threshold, the plasma formed by ac breakdown cuts off transmission in about 100 psec. The entire shutter assembly is also shielded.

After truncation, the polarization of the pump pulse is rotated and the pulse is weakly focused into the CH_3F cell, which consists of 1.68 to 10.21 m of 38-mm Pyrex tubing with an "input coupler" on either end. These couplers are multilayer dielectric-coated silicon Brewster windows[58] which reflect the ir and transmit the FIR with minimal loss. The pressure of CH_3F in the cell is monitored by a capacitive manometer. After exiting the cell, the pump pulse is focused through an attenuating film of black polyethylene (for feedback reduction) onto a germanium photon drag detector with a nanosecond response time. The FIR is filtered to remove stray ir and is weakly focused through a high-density polyethylene window onto a fast phosphorus-doped-silicon photoconductor[59] which is cooled to approximately 2.5 K.

C. Procedure

It was necessary to have smooth, intense, repeatable CO_2 laser pulses with a fast rise time in order to make the truncated pulse as short and jitter free as possible. Careful laser adjustment resulted in a smooth pulse that could be truncated to a full width at half maximum (FWHM) of 15 nsec. This truncated pulse had an energy of 14 mJ, and jitter in the cutoff time was less than 1 nsec. However, this and other factors caused the transverse intensity profile of the pump not to be purely Gaussian; the profile deviated above the Gaussian away from the beam axis. The transverse profile was determined at several points inside the range of cell lengths by measuring the transmission of a variable-diameter aperture.

The absence of ir and FIR feedback was verified and, for several cell lengths, the FIR polarization (relative to that of the pump) was measured for the forward and backward waves at various CH_3F pressures by measuring the transmission of a grating polarizer. In addition, for a similar set of cell lengths and CH_3F pressures, the effects of lengthening the pump pulse (by means of a delayed cutoff) were investigated. Then for seven cell lengths from 168 to 1021 cm, oscilloscope traces of five or more superradiant and pump pulses were photographed.[60] This was done for at least ten pressures at each cell length for both forward and backward emission.

D. Results

Representative pump (upper trace) and forward superradiant pulses are shown in Fig. 3. The pump intensity varies nearly quadratically with time before cutoff; the fall time observed is that of the pulse amplifier, not the plasma shutter. The pump and FIR, recorded on alternate traces, are synchronized to within a nanosecond. In Fig. 3 are seen (a) an example of a nearly sech^2 superradiant pulse, (b) one of the shortest superradiant pulses observed with a width (FWHM) of 14 nsec and a less regular shape, and (c) a multiple exposure of ten shots, displaying five pump and five superradiant pulses, and showing the shot-to-shot fluctuation observed. Note the shape of the FIR pulses in Fig. 3(c); they are not sech^2, and they do not quite exhibit ringing. This has an explanation in terms of parallel transitions, as will be discussed. None of these superradiant pulses overlaps the pump, and the results to be given include

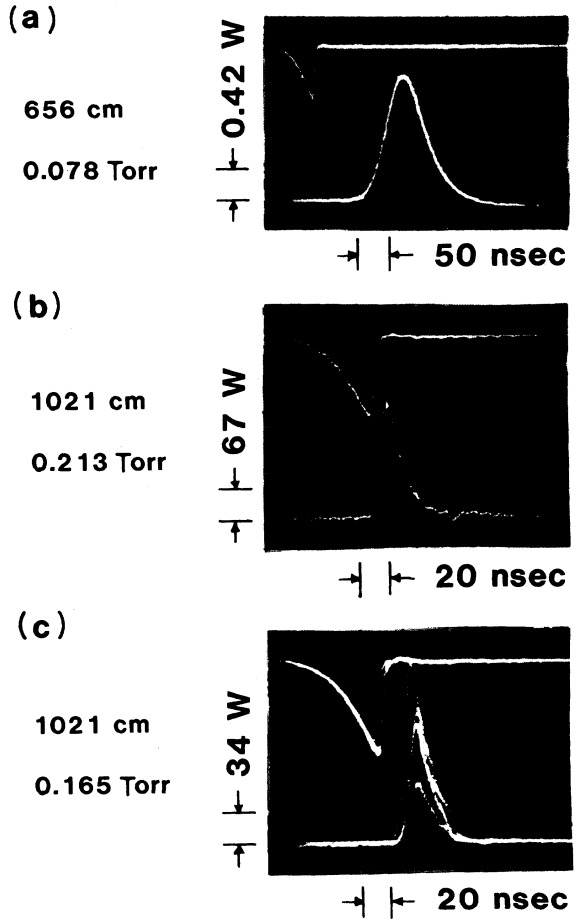

FIG. 3. Typical pulses, showing (a) superradiant pulse shape, with overshoot on trailing edge due to pulse amplifier; (b) a short superradaiant pulse without overshoot (amplifier was not used); (c) multiple exposure showing shot-to-shot fluctuation. In each case, the upper pulse is the truncated pump pulse and the vertical scale applies only to the FIR superradiant pulse.

no overlapping pulses, even though some of these seemed to indicate that the superradiant evolution could proceed unperturbed by the trailing edge of the pump pulse.

The dependence of the forward superradiant pulse parameters on pressure (hence on N) (Ref. 61) is shown in Figs. 4–7 for four cell lengths from 168 to 1021 cm. Each point plotted in these figures represents an average[62] of five or more pulses. The lines in these figures are linear least-square fits to the data within specific ranges of pressure. In Fig. 4, for a 168-cm cell, the delay and width vary linearly with inverse pressure, characteristic of superradiant emission. The delay, measured from pump cutoff, has a high-pressure limit of -22 nsec; this reflects the finite width of the pump pulse.[63] The intensity data are not inconsistent with a linear dependence on pressure squared, but it appears that different slopes may be obtained for low pressures and high pressures; the break, at $p^2 \simeq 0.01$ Torr^2, becomes more pronounced for longer cells. Fig. 5 (351 cm) shows similar behavior, including the same negative delay intercept and break in intensity dependence. There is less scatter in the data from this longer cell, because of smaller fluctuations. For this and longer cells, all superradiant pulses have widths less than the dominant relaxation time T_2. Figure 6 shows the same qualitative behavior for the pulses from a 656-cm cell, but now breaks are apparent in the delay and width plots as well. These breaks occur near 0.07 Torr, approximately the same pressure as that where the break occurs in the intensity dependence. This pattern is repeated in the data from a sample of length 1021 cm (Fig.7), all breaks occuring in the pressure range from 0.06 to 0.10 Torr.

From the data, the constant-pressure pulse parameter dependence on sample length has been determined. This allows comparison of the power-law (L^m) dependence of the pulse width, delay, and intensity with that which is predicted by mean-field theory. It is found that for the delay and the width, m seems to lie between -0.5 and -1.5, with the dependence becoming stronger as cell

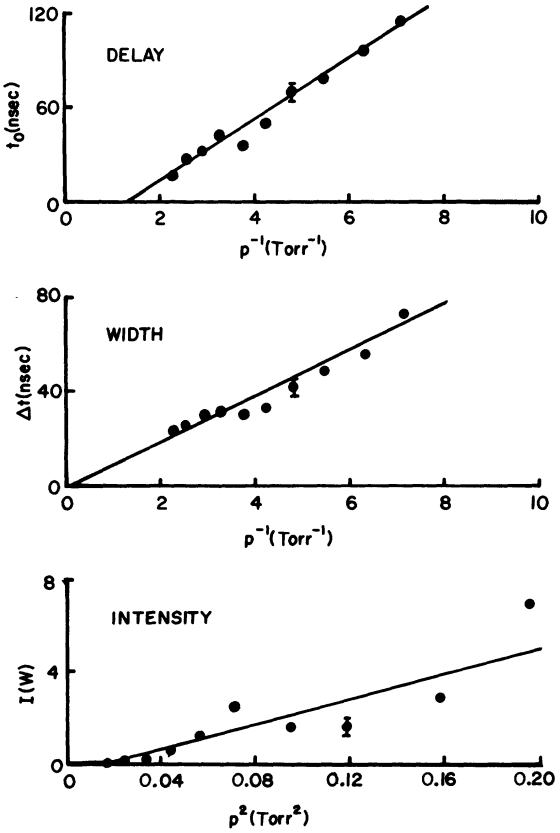

FIG. 4. Pressure dependence of the superradiant pulse parameters: forward emission, 168-cm CH_3F cell. The error bars in this and following figures represent the average fluctuation rather than the uncertainties of the means.

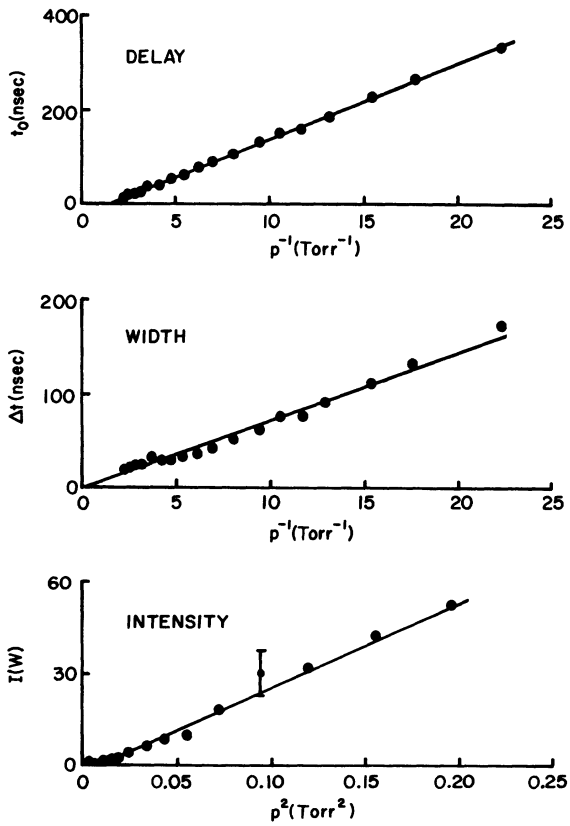

FIG. 5. Pressure dependence of the superradiant pulse parameters: forward emission, 351-cm CH_3F cell.

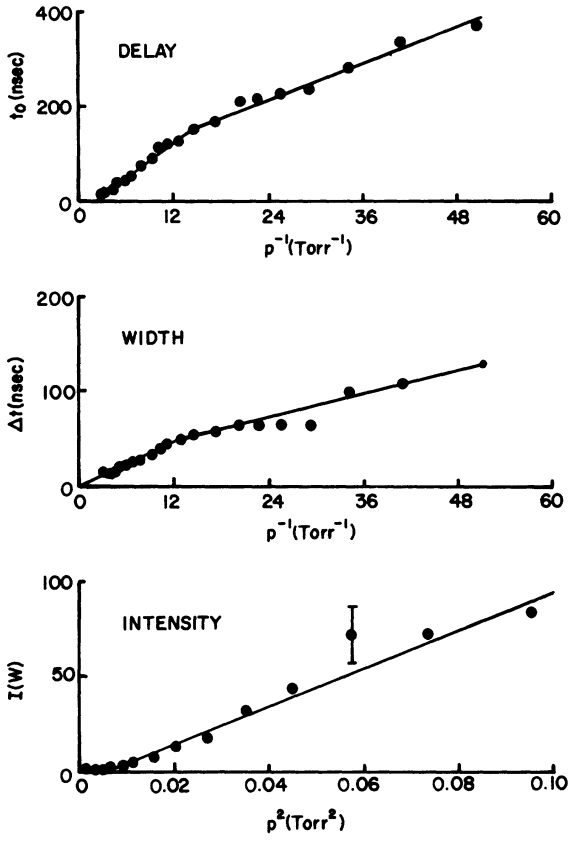

FIG. 6. Pressure dependence of the superradiant pulse parameters: forward emission, 656-cm CH_3F cell.

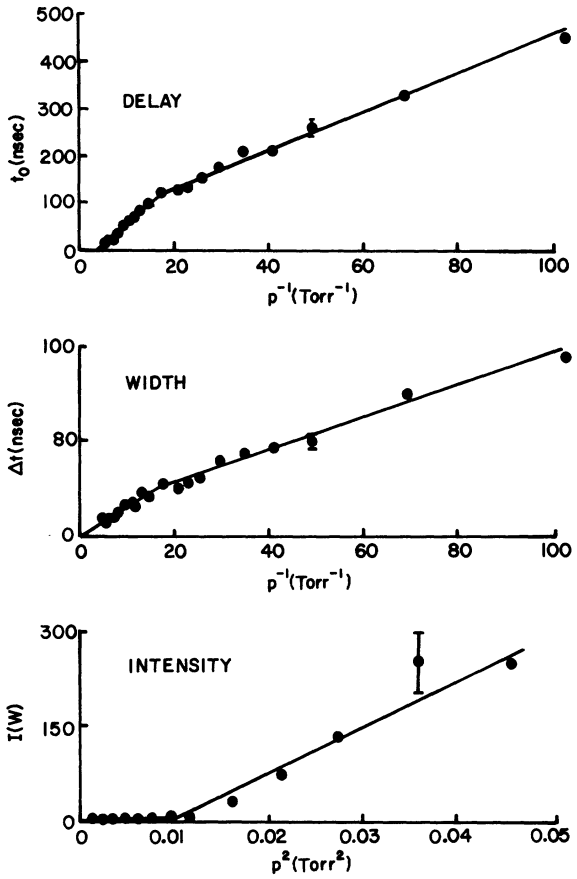

FIG. 7. Pressure dependence of the superradiant pulse parameters: forward emission, 1021-cm CH_3F cell.

length increases. For the intensity, m lies between 3 and 4 and decreases with increasing L.

The dependences of the pulse parameters on pressure and on cell length were also studied for backward emission. For cell lengths less than 5 m the pressure dependences are qualitatively the same as for forward emission, with breaks in the slopes occuring in the same pressure range as noted in Figs. 4–7. In the case of the shortest cell, the backward-wave data are quantitatively the same as the forward-wave data, within our experimental uncertainties. For cells longer than 5 m, there is a significant qualitative difference from the forward-wave results; the broken-linear behavior becomes more complex. This may be due to the onset of swept-gain superradiance in the longer samples. For reasons which are not well understood, it was much more difficult to measure the backward-wave characteristics, resulting in uncertainties large enough to preclude a determination of the true shapes of the pressure-dependence curves. The delay and width were much less sensitive to cell length than were those of the forward pulses, but the backward pulse intensity showed a rather erratic L dependence.

In spite of the large uncertainty in the backward pulse intensity, it is interesting to consider the behavior of the forward-backward intensity ratio R. The criterion which has been proposed[42] to distinguish swept-gain superradiance from Dicke superradiance is the increase of R from unity. In Fig. 8, R is plotted as a function of pressure for two cell lengths and as a function of cell length for two pressures. It appears that R is significantly greater than one for pressures above 0.1 Torr and cell lengths greater than 5 m, but the large uncertainties in R make quantitative conclusions problematic. However, we can say that R is large compared to unity for high pressures in our longer cells, and claim that this is a likely indication of the onset of swept-gain superradiance.

The relative polarization of the FIR emission was found to be approximately 3:1, polarization perpendicular to that of the pump being favored over parallel polarization. The values found ranged from 1.5:1 to 5:1, with no strong dependence

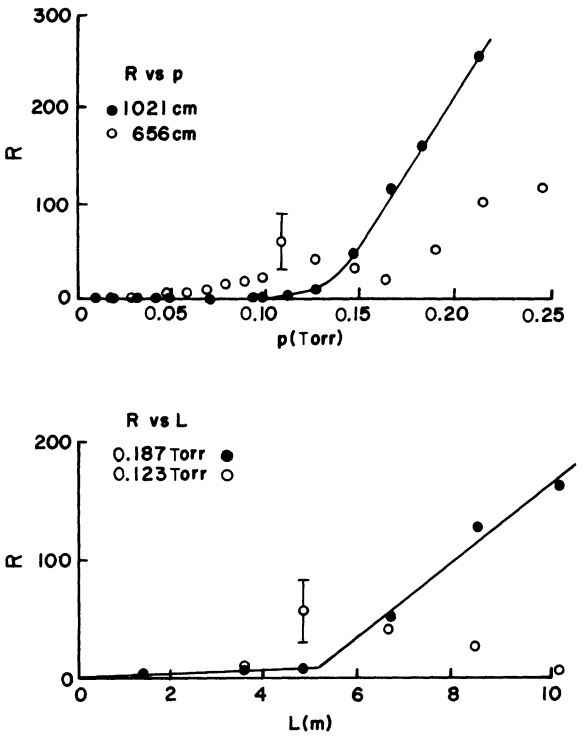

FIG. 8. Forward-backward peak intensity ratio $R = I_F/I_B$ as a function of pressure for two cell lengths and as a function of cell length for two pressures.

on cell length or pressure. This contrasts with the polarization ratio expected from stimulated emission, which would be much larger. This is indicative of the characterization of the process as a "noise-driven amplifier,"[27] rather than as a noise (spontaneous emission) amplifier, and this will be discussed in the next section in terms of level degeneracy and pump efficiency. Varying the pump duration by delaying the plasma-shutter cutoff (by 5–20 nsec) had little effect on the superradiant pulses, other than in the delay. This further supports the conclusion that the negative delay intercept is due to the finite width of the pump pulse.[63] This will also be discussed in more detail later.

III. SEMICLASSICAL MODEL

A. Maxwell-Bloch equations

Because the excitation was swept in our experiment, it was considered necessary to treat propagation explicitly; to this end, the semiclassical approach was used. Since the coherent interaction of the ir and FIR was estimated to be relatively weak, these two-level systems were taken to be independent except for the incoherent effects noted below. It was felt that their coherent interaction could be approximately taken into account by proper calculation of the FIR initial condition.[63] Each two-level system could then be described by the Maxwell-Bloch equations,[32] which, for a bidirectional plane wave in the rotating-wave and slowly varying amplitude and phase approximations, take the form

$$\frac{\partial}{\partial t} n = -\frac{1}{T_1}(n - n_e) - \frac{1}{\hbar}\,\mathrm{Re}(E_1 P_1^* + E_2 P_2^* + E_1 P_2^* e^{-i2kx} + E_2 P_1^* e^{i2kx}), \tag{1a}$$

$$\frac{\partial}{\partial t} P_1 = -\left(\frac{1}{T_2} + i\Delta\right) P_1 + \frac{\mu_{12}^2}{\hbar} n E_1, \tag{1b}$$

$$\frac{\partial}{\partial t} P_2 = -\left(\frac{1}{T_2} + i\Delta\right) P_2 + \frac{\mu_{12}^2}{\hbar} n E_2, \tag{1c}$$

$$\left(\frac{\partial}{\partial x} + \frac{1}{c}\frac{\partial}{\partial t}\right) E_1 = -\kappa E_1 + 2\pi k P_1, \tag{1d}$$

$$\left(-\frac{\partial}{\partial x} + \frac{1}{c}\frac{\partial}{\partial t}\right) E_2 = -\kappa E_2 + 2\pi k P_2. \tag{1e}$$

In Eqs. (1), n is the population density difference, $n_2 - n_1$, between levels 2 (upper) and 1 (lower). T_1 and T_2 are, respectively, the longitudinal and transverse relaxation times. The equilibrium population density difference is n_e, and $\Delta(=\omega - \omega_0)$ is the field detuning from molecular resonance. The physical field and polarization (z components) are given in terms of their complex amplitudes, E_i and P_i by

$$E(x,t) = \mathrm{Re}\left[E_1(x,t)e^{i(\omega t - kx)} + E_2(x,t)e^{i(\omega t + kx)}\right], \tag{2a}$$

$$P(x,t) = \mathrm{Re}\left[iP_1(x,t)e^{i(\omega t - kx)} + iP_2(x,t)e^{i(\omega t + kx)}\right]. \tag{2b}$$

Here k is the wave number ($=2\pi/\lambda$) also appearing in Eqs. (1a), (1d), and (1e). A linear loss term is added to the wave equations (1d) and (1e) to approximate diffraction. The constant κ is taken to be[24]

$$\kappa = \frac{1}{2L}\ln\left[1 + \left(\frac{\lambda L}{A}\right)^2\right], \tag{3}$$

where A is the cross-sectional area of the cylinder of excited molecules and the emission is treated as a far-field Gaussian beam. The coupling between field and polarization takes place through the (z-component) electric dipole moment matrix element, μ_{12}, in Eqs. (1b) and (1c). It should be noted that in the proper limits of Eqs. (1), the mean-field results[19] can be recovered, as can the

pendulum equation,[19] the swept-gain results,[28] and the small-pulse solution.[24]

In order to use Eqs. (1) to attempt to describe our experiment, several modifications must be made. For both the pump absorption and the FIR emission, the M degeneracy of the states involved must be taken into account, as well as the (optical) polarizations. Doppler broadening must also be included for the pump absorption. Treating the absorption and emission independently requires that a source term for n must be included in the FIR equations. Also necessary will be a source of polarization (P), including fluctuations, as an initial condition for the FIR emission. The Maxwell-Bloch equations will then be solved separately for each value of K labeling a possible parallel transition.

B. Numerical model

Consider first the absorption: Because the pump is intense enough so that relatively little of it is absorbed, we make the approximation of neglecting the wave equation; the pump field is nearly independent of x. In terms of retarded time $t' = t - x/c$, the Bloch equations used are then

$$\frac{\partial}{\partial t} n_p = -\frac{1}{T_1}(n_p - n_{pe}) - \frac{1}{\hbar}\mathrm{Re}(E_p P_p^*), \tag{4a}$$

$$\frac{\partial}{\partial t} P_p = -\left(\frac{1}{T_2} + i\Delta_p\right) P_p + \frac{\mu_{02}^2}{\hbar} n_p E_p . \tag{4b}$$

The prime on t has been dropped and the subscript p implies pump. Degeneracy and Doppler broadening are included, as n_p and P_p are understood to pertain to specific values of magnetic quantum number M and velocity. The equilibrium (and initial) population density difference n_{pe} is the negative of the ground state (labeled 0) population density. The pump field is taken, to a very good approximation, to be a real linear function of retarded time from 0 to 55 nsec and zero elsewhere. The detuning Δ_p includes both pump offset (Δ_a in Table II) and velocity detuning. The squared dipole matrix element is given by

$$\mu_{02}^2(M) = \mu_{ir}^2 \frac{K^2 M^2}{J^2(J+1)^2}, \tag{5}$$

where J is the value of the rotational quantum number of the upper level (labeled 2). Use of Eqs. (4) and (5) implies that the selection rule $\Delta M = 0$ is obeyed, and this results from taking the quantization axis parallel to the electric field of the linearly polarized pump.

Using initial conditions $n_p(t=0) = n_{pe}$ and $P_p(t=0) = 0$, Eqs. (4) are solved using a second-order Runge-Kutta or predictor-corrector method. The solution $n_p(\Delta_p, M, t)$ is then integrated over velocity detuning using Hermite-Gaussian quadrature, and the FIR population density source term is calculated, for each M, as a function of time for the duration of the pump. The average over velocity is justified by the fact that the FIR is influenced only weakly by Doppler broadening, even at the lowest pressures.

Because of the large experimental uncertainties in the backward-pulse characteristics and the high cost of including both degeneracy and bidirectional emission in the FIR calculation, unidirectional (forward) emission alone was calculated. Bidirectional calculations without degeneracy indicated that the forward-backward coupling was small, making this a good approximation. Including the source terms, the Maxwell-Bloch equations take the form (t is retarded time)

$$\frac{\partial}{\partial t} n = S - \frac{1}{T_1}(n - n_e) - \frac{1}{\hbar}\mathrm{Re}(EP^*), \tag{6a}$$

$$\frac{\partial}{\partial t} P = U - \frac{1}{T_2} P + \frac{\mu_{12}^2}{\hbar} n E, \tag{6b}$$

$$\frac{\partial}{\partial x} E = -\kappa E + 2\pi k \sum_M P, \tag{6c}$$

where n and P depend on M. The polarization source was calculated so that the polarization initially created depended on the initial population density in the following way:

$$P_i(M, t) = \int_0^t U(M, t')dt'$$

$$= \mu_{12}(M) n_i(M, t) \sin\theta_0, \tag{7a}$$

where

$$n_i(M, t) = \int_0^t S(M, t')dt', \tag{7b}$$

and θ_0 is a quasifree parameter (initial tipping angle) discussed in more detail in the Appendix. The equilibrium population density difference is determined by rotational relaxation alone; the emission is over before other relaxation processes can contribute significantly. The square of the dipole matrix element depends on M as follows ($\Delta M = 0$):

$$\mu_{12}^2(M) = \mu^2 \frac{(J^2 - K^2)(J^2 - M^2)}{J^2(4J^2 - 1)}, \tag{8}$$

where J again pertains to the upper level. This is for emission polarized parallel to the quantization axis, that is, parallel to the pump polarization. In order to calculate emission of the orthogonal

polarization, the axis of quantization was rotated according to the Wigner formula.[64] This resulted in a different functional dependence of S and U on M (in the new reference frame), and the same Eqs. (6) could be used.

These equations were also solved by the predictor-corrector technique, which has been shown to give a stable solution.[32] The output of the computer program included $n(M, x, t)$, $P(M, x, t)$, and $E(x, t)$ for fixed M and t, FIR intensity $I(x=L, t)$, and the McCall-Hahn area of the emitted pulse. The fraction of the ground-state population excited for each M, as a function of time, was also included in the output. (The program was checked by reproducing the results of Ref. 24.) The input was determined by experimental conditions, with the FIR cross-sectional area estimated (based on numerical results) to be equal to the pump spot size averaged over cell length. This area is given in Table III, along with the estimated diffraction loss, the Fresnel number, and the excited population density.

As noted in the Introduction, many details of the excitation and emission processes must be included to allow a fit of the numerical results to the data over the full range of cell lengths and pressures. For reference purposes, the relative sensitivity of the calculated parameters to variations in certain input variables is compiled in Table IV. Careful note should be made that the indicated sensitivity is for a fixed length and pressure only. Two particularly interesting results are the strong sensitivity to the collisional relaxation rate and the smaller ratio of delay variation to intensity variation for changes in T_2.

C. Numerical results and comparison with experiment

Figure 9(a) shows the reason for a preferential linear polarization of the FIR perpendicular to that of the pump. There, the calculated fraction of the initial ground-state population excited by the pump is plotted versus M in the original and rotated reference frames. The pump is a Q-branch transition, so the excited population distribution in the original frame is weighted in favor of large M [see Eq. (5)]. When the quantization axis is rotated, this distribution becomes more uniform and weighted in favor of small M Since the FIR emission is R branch, its transition matrix element [Eq. (8)] is greater for small M. The perpendicularly polarized emission will therefore be favored.

Fig. 9(b) shows the calculated effect of Doppler broadening on the excitation process for large and small M and for the total population. Partial co-

TABLE III. Effective sample dimensions, linear loss, Fresnel number, and density of excited molecules.

L (cm)	A (cm^2)	κ (10^{-3} cm^{-1})	F[a]	n (10^{13} cm^{-3})[b]
168	2.08	8.44	0.50	7.22
229	1.88	7.91	0.33	7.27
351	1.55	6.90	0.18	7.51
473	1.29	6.14	0.11	7.75
656	1.04	5.25	0.06	8.00
838	0.95	4.51	0.05	7.82
1021	1.03	3.82	0.04	8.00

[a] $F=2A/\lambda L$.
[b] For $K=2$, $p=0.144$ Torr.

TABLE IV. Effect of input parameter variation on calculated output pulse characteristics.[a]

Parameter	Variation	Resultant variation in I	Δt	t_0
Tipping angle θ_0	25–200%[b]	20%	10%	10%
Loss κ	15%	20%	10%	10%
Relaxation time T_2	5%	20%	10%	3%

[a] Results apply to a typical single point: cell length (L) and CH_3F pressure (p) fixed.
[b] The results are markedly less sensitive to θ_0 as L and p increase.

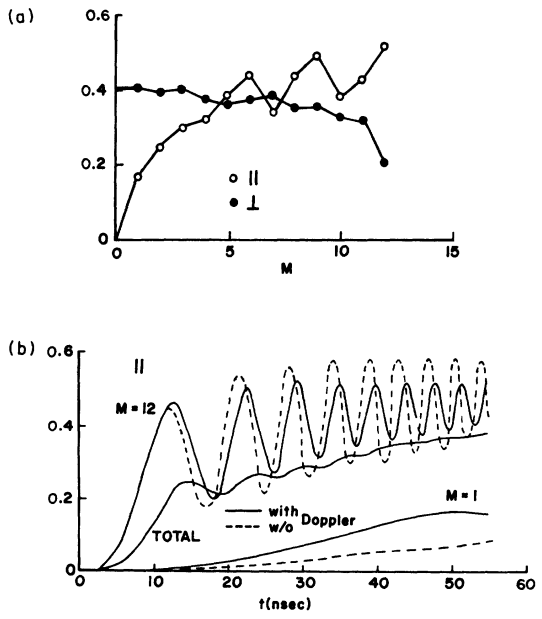

FIG. 9. (a) Population fraction excited, by M sublevel. Open points indicate the parallel polarization, solid dots the perpendicular one (in the orthogonal reference frame). (b) Effect of Doppler broadening and degeneracy on Rabi oscillations of excited fraction, for $M=1$ and 12 and for the total population.

herence of the pump is evident in the presence of Rabi oscillations for $M = 12$; Doppler broadening helps to damp these oscillations faster than collisional dephasing alone. The effect on $M = 1$ is also shown for comparison. Averaging over all M with Doppler broadening included, the differing oscillations nearly cancel. Since different-M cases are treated as evolving independently, however, the partial coherence of the pump should be taken into account.

This is done by noting that the initial evolution of the Bloch angle $\theta(t)$ reflects the width of the pump pulse and the possibility of coherent (Raman) effects which would create an initial FIR polarization. This is discussed in the Appendix, where the initial tipping angle is given as

$$\theta_0 = 0.35\frac{2}{\sqrt{N}} = G\theta_{0e}. \tag{9}$$

In Eq. (9), the expected initial tipping angle is given by

$$\theta_{0e} = 0.03\frac{2}{\sqrt{N}}, \tag{10}$$

calculated as in Ref. 24; this method takes into account the bandwidth narrowing that occurs in high-gain systems and includes the contribution of thermal (blackbody) radiation to the tipping angle. G is a scaling factor which may be considered a free parameter. A proper choice of G permitted a quantitative fit to all our experimental results.

This fit was more effective as cell length increased. The two worst cases were those for $L = 168$ cm and $L = 229$ cm; the latter is shown in Fig. 10. In this figure the solid lines are theoretical predictions for the single choice of G which gives the best fit over all cell lengths. Theory and experiment are seen to agree fairly well even in the worst case. Similar plots for other cell lengths would be practically indistinguishable from Figs. 5–7 and so are not shown. Figure 11 shows how well the superradiant pulse shape is reproduced by the calculation. All calculations have been done in the rotated frame because the cell's Brewster-angle output coupler preferentially passes perpendicularly polarized FIR. In these short cells (Figs. 10 and 11), only the transitions with $K = 2$ are found to contribute. To fit the experimental data from longer samples, $K = 1$ and $K = 3$ transitions must be included.[65] Figure 12 shows two examples. The slight shoulder on the upper experimental pulse is explained by the influence of the $K = 3$ emission. In the lower pulse, the three single-K pulses overlap to give a smooth but asymmetric pulse.

The breaks in the linear dependences of the pulse parameters noted in Figs. 4–7 occur in the range

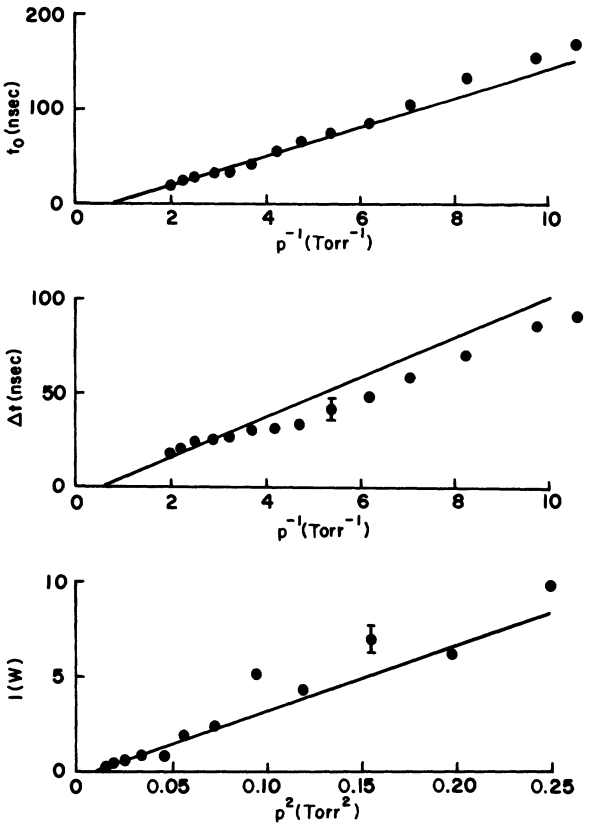

FIG. 10. Semiclassical fit (lines) to experimental points 229-cm cell, forward wave.

where Doppler broadening might begin to appear as a line broadening in the FIR. However, the lines would break the other way if the change in the dominant line-broadening mechanism were the cause of this behavior. In fact, Doppler broadening is not included in the calculation because we found separately that doing so had negligible effect on the results, even at very low pressures. It is be-

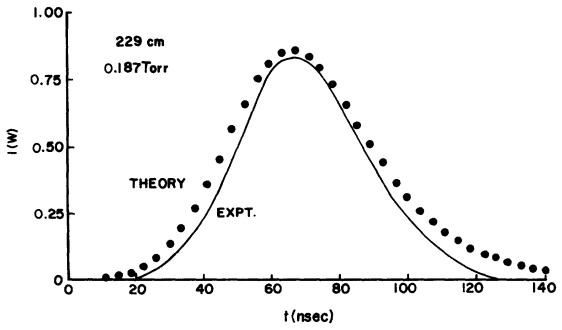

FIG. 11. Comparison of the observed (solid line) and calculated (dots) superradiant pulse shape; $p = 0.187$ Torr, $L = 229$ cm.

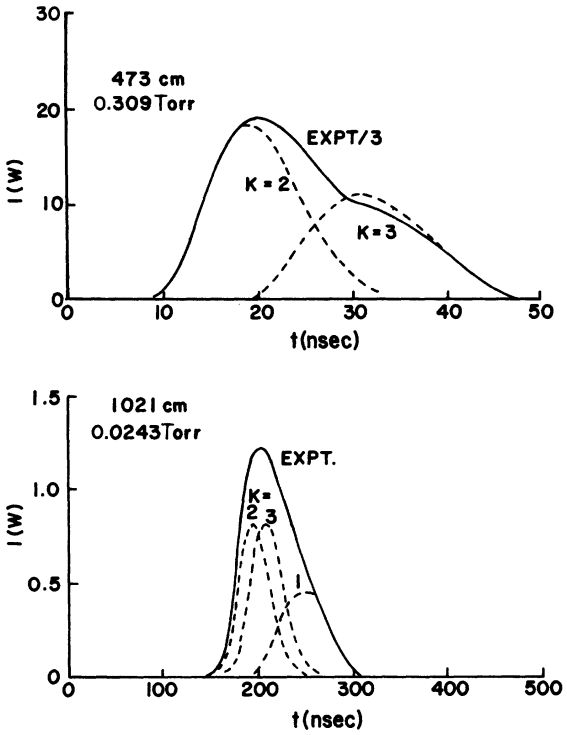

FIG. 12. Semiclassical fits (broken lines) to observed pusles (solid lines), in cases where two (top) and three (bottom) K emissions must be combined to give a reproduction of the data. In the upper case, the experimental pulse requires a threefold reduction in order to achieve a quantitative fit to the calculated intensity. This was the case for some of the data from the 473-cm cell and may have been due to miscalibration of an attenuator.

lieved that the breaks may be due to a change in the interaction of the different K emissions from coherent to incoherent as the pressure is decreased. At high pressures, the time scale for the onset of cooperation [a few T_R as given in Eq. (A3)] is short enough that the corresponding frequency spread will overlap at least the $K=2$, 3 transitions. These different systems will therefore evolve together in phase, approximately doubling the number of cooperating molecules. As the pressure decreases, the pulse time scale becomes long implying a narrower spectrum which eventually reaches a point where the K transitions evolve independently. The frequency separation of the different K transitions (Table II) and the calculated value of T_R give a transition pressure which agrees with the observed value.

When fluctuation is introduced into the calculation by assigning a randomly varying space-dependent phase to the initial FIR polarization P_i, a fluctuation in the superradiant pulse intensity is predicted. This varies from ±50% to ±10% as cell length increases in the experimental range. Corresponding fluctuations in the delay and pulse width are predicted to vary from ±10% to ±2%. This is the same order as the observed shot-to-shot fluctuation, but similar results could be caused by variations in pump frequency and radial intensity profile. Calculations show that the pump-frequency fluctuation, expected to be a few MHz, will produce fluctuations in the superradiant pulses as large as those observed. We therefore cannot claim that the observed fluctuations result from quantum noise.

The calculated polarization ratio for the FIR ranged from 100 to 2 as the length of the cell increased; it seemed to be very sensitive to cell length and to pump intensity. The observed range was 5 to 1.5. The lack of agreement may be due to an overestimate of the cross-sectional area (hence an underestimate of the pump intensity) in the shorter cells. This may also explain the relatively poorer fit to the pulse parameters achieved for the shorter cells.

The experimental and calculated length dependence of the pulse parameters agree. They both disagree with mean-field theory, which predicts dependence of delay and width as L^{-1} and of intensity as L^2 in the disk limit ($F>1$), and dependence of intensity as L and L-independent delay and width in the needle limit ($F<0.1$). Taking the values of F from Table III, the disagreement is obvious (cf. Sec. II D), but comparison is hampered by the fact that A also depends on L. This disagreement supports the conclusion that propagation is an important effect, and that swept-gain superradiance may be of importance for the longer cells. As independent support of this, we have also noted that the spatial growth of the intensity for short cells scaled as $\exp(\sqrt{L})$ which is characteristic of small area, swept gain, lethargic, superradiant, and stimulated Raman emission systems.[27,28]

IV. CONCLUSIONS

The calculations support our claim that the effect that we have observed in the far-infrared emission from optically pumped methyl fluoride is superradiance. This is evidenced in the behavior of the pulse parameters as N is varied. Whether the emission is superfluorescent, that is, evolved from full inversion, is another question. Based on the semiempirical value of the initial tipping angle, we believe that it is not; the swept excitation and the observation of asymmetric emission also support this opinion. We observed no ringing; the calculations suggest that the reason for this was either the small fraction excited (~0.35) or the

large rotational relaxation rate. Some pulses exhibited structure, as the upper one in Fig. 12, but this is a result of the presence of several nearly independent superradiant transitions. Ringing predicted by our calculations when the density or T_2 was artifically increased was of the Burnham-Chiao[66] type, as calculated in Ref. 24. This type of ringing has not been observed in superradiance experiments, except perhaps in HF (Refs. 33 and 24).

Some aspects of the comparison of calculation with experiment deserve further discussion. First, it must be pointed out that N is not directly measured but, rather, calculated from the interaction of the pump with the ir transition. This depends on pump intensity somewhat, and hence on the estimate for the cross-sectional area of the beam. It will also depend on the damped Rabi oscillation of each M subtransition. Even considering these possible complications, it is felt that N is known to within 10%, or perhaps 20% for the worst cases. Another uncertainty is that of the values of T_1 and T_2. Since homogeneous broadening is dominant in our experiment, it is important to know these rotational relaxation times as accurately as possible. They have been measured, however, only for low-J transitions in CH_3F; comparison with the calculations of Murphy and Boggs[47] for methyl chloride suggests that the measured T_1 and T_2 should be taken to have uncertainty of ten to twenty percent when applied to our high-J transition. This is supported by the results of Hodges *et al.*[49] and by our observation of the effect of introducing helium into the cell to enhance relaxation and dephasing.[67] We observed a relatively small change in delay while the intensity was substantially reduced, both in accord with the calculated behavior in Table IV.

The importance of including degeneracy in the calculation is seen in the effect of the pump and in the relative polarization of the FIR. Some of the approximations made should be examined, however. The pump was assumed to be negligibly depleted by absorption; this is a good assumption except possibly for the longest samples at their highest pressures. In those cases, separate calculations show small effect of a weakened pump on our major results. An assumption is made in calculating the perpendicular and parallel emission separately; this is supposed possible because one results mainly from high-M transitions and the other mainly from low-M transitions. The two will, however, overlap to some degree, possibly explaining the disagreement between the theoretical and experimental relative FIR polarizations. In addition, the three absorption-emission processes for different values of K are treated independently. This neglects the possibility of coherent interactions, but the effect of this on the determination of the initial tipping angle would be reduced due to the apparent T_R dependence of the initial condition (see Appendix). The net effect would not be large enough to change the order of magnitude determined for θ_0, since the effective N would increase by at most a factor of two.

Coherent effects of the pump have been included only implicitly, in the semiempirical value of θ_0, where the effects of blackbody radiation and gain narrowing have been included in an overall factor, as suggested by Ref. 24; their effects, however, may be unimportant if the initial condition is determined by Raman scattering. Our semiempirical value of the initial tipping angle suggests better agreement with $N^{-1/2}$ dependence than with the $(\mu N)^{-1/2}$ dependence, but our results should not be considered conclusive in light of the difficulty of properly defining the initial condition in our experiment.

The beginning of the transition from Dicke superradiance to swept superradiance is observed and agrees with the qualitative predictions of the simpler model in which degeneracy is ignored. This conclusion is also supported by the small Fresnel numbers of the long samples and the fact that these samples are many cooperation lengths long. Another geometrical problem is that of the observed shot-to-shot fluctuations, which are probably due to laser frequency variation and transverse mode instability. The entire question of transverse effects is one which had to be ignored except in the calculation of the cross-sectional area A and in estimation of the resultant fluctuations and of the diffraction loss κ. The form of the dependence of the delay on $\ln N$ is thought to be either linear or quadratic. Because the dependence is so weak and because of the uncertainty in N, we are unable to distinguish between these two possibilities. The calculation shows that even a single-K emission pulse can have a McCall-Hahn area greater than π. This may be an argument for the existence of a time-varying emission frequency, or chirp.[68] This would not be surprising, as even a simple model predicts a chirp.[22]

To summarize, our observation of superradiance is in the homogeneously broadened regime, and the effect of transition to the Doppler-broadened regime was not seen even at our lowest pressures. This is due to the relatively much greater effect of homogeneous broadening on the superradiant emission, which is evident even in the HF experiment results. The transiton from Dicke superradiance to swept superradiance is observed to begin to take place in long samples at high densi-

ties. The predicted steady state,[27,28] however, is not achieved; we estimate that a cell perhaps three times as long (~30 m) would be needed to approach steady state with a 15-nsec pump pulse width. In comparing the Maxwell-Bloch predictions with the data, it is found necessary to include the pump process in detail, including the shape and duration of the pump, its polarization, and the degeneracy and Doppler broadening of the absorbing transition. It is also found necessary to include degeneracy in the FIR emission calculation to account for the proper behavior and polarization of the superradiant pulses. In addition, as many as three parallel transitions (different values of K) must be included to reproduce the experimental results. However, all our forward-wave data can be reproduced quantitatively by the choice of one free parameter (G) in the expression for the initial condition.

Finally, aside from the fundamental interest in superradiant systems, the practicalities of employing this effect for the generation of ultrashort far infrared pulses can be commented on. First, using the analytical results for the steady-state superradiant pulse intensity in Ref. 28, the maximum pulse energy expressed as a fraction of the initial energy stored in the upper level scales as $(\kappa x)^{-1}$. Since κx values of greater than ten are needed to reach the steady state, the pulse energy extraction efficiency is less than 10% which should be compared with a normal pulsed laser efficiency of 50%. In the steady state, the peak pulse intensity and pulse duration are expected to be ~10 kW/cm^2 and ~200 psec for methyl fluoride at ~1 Torr. Recent experiments utilizing a mode-locked train of pumping pulses have resulted in the generation of a train of sub-T_2 pulses from methyl fluoride and other gases.[69,70] In particular, pulse durations of $< T_2/10$ or between 400–800 psec and peak pulse intensitites of > 10 kW/cm^2 were observed which compares favorably to single pulse superradiance but obtainable in shorter distances, a few meters. The relationship between these latter experiments and multipulse swept gain superradiance and stimulated raman emission will be addressed later.[71]

ACKNOWLEDGMENTS

The authors wish to thank Dr. Sam Petuchowski for his contributions to the earlier phases of this work, Dr. Paul Norton for loan of the Si:P detector, Dr. E. A. Jung for providing plans and parts for the Marx bank pulser, and Dr. R. Bonifacio, Dr. C. Bowden, Dr. J. Eberly, Dr. M. Feld, Dr. H. Gibbs, Dr. F. Hopf, and Dr. L. Narducci for spirited discussions. This work was supported in part by the Army Research Office through Grants Nos. DAHC-04-75-C-0099 and DAAG 29-78-C-0128, and in part by the Research Board and Industrial Affiliates Program of the University of Illinois.

APPENDIX

According to the method of Ref. 24 for calculating the effective initial tipping angle for an inverted system, we calculate an expected initial angle of

$$\theta_{0e} = 0.03 \frac{2}{\sqrt{N}}. \tag{A1}$$

As usual, N is the number of excited molecules; the multiplying factor is a constant here because we are in the homogeneous limit.

Use of the form of θ_0 given above, however, is warranted only if the exciting pulse is of negligible duration. If this is not the case, the Bloch angle will evolve during the pump pulse[63]:

$$\theta(t) = \theta_{0e} \sin\left[\frac{\omega_R t}{2}\right] \exp\left[\frac{t}{4T_R} - e^{-t/2T_2}\frac{\sin\omega_R t}{4\omega_R T_R} - \frac{1}{\omega_R T_2}(1 - e^{-t/2T_2}\cos\omega_R t)\right]. \tag{A2}$$

Here, the superradiance time T_R is given by

$$T_R = 8\pi A T_{sp}/\lambda^2 N, \tag{A3}$$

where T_{sp} is the spontaneous lifetime as in Table II; ω_R is the pump Rabi frequency,

$$\omega_R = \mu_{02}(M)E_p/\hbar. \tag{A4}$$

The above assumes a pump of constant intensity.

Because the time evolution of the tipping angle takes a different form in the presence of the pump, the initial value θ_0 which must be used as input for the numerical solution will appear to depend on T_R and x (ω_R depends on x because the pump is weakly focused into the cell). Extracting this dependence, according to Equation (A2), by choosing a time-independent equivalent ω_R and averaging over M results in the following value for the initial tipping angle:

$$\theta_0 = 0.35 \frac{2}{\sqrt{N}}. \tag{A5}$$

This is to be understood as the tipping angle which would be produced by a delta-function π-pulse pump. Comparison with (A1) shows that this is approximately ten times the value expected from Ref. 24. This single factor of 10 allows a fit to our data for all cell lengths and pressures.

*Present address: Department of Physics, Western Illinois University, Macomb, Illinois 61455.
[1]R. H. Dicke, Phys. Rev. 93, 99 (1954).
[2]Over one hundred papers have been published on superradiance theory; the following is not intended to be an exhaustive listing, but rather a collection of those which have had the greatest influence on our work. Several papers not published elsewhere can be found in *Cooperative Effects in Matter and Radiation*, edited by C. M. Bowden, D. W. Howgate, and H. R. Robl (Plenum, New York, 1977), and in Ref. 3.
[3]*Coherence and Quantum Optics IV*, edited by L. Mandel and E. Wolf (Plenum, New York, 1978).
[4]V. Ernst and P. Stehle, Phys. Rev. 176, 1456 (1968).
[5]N. E. Rehler and J. H. Eberly, Phys. Rev. A 3, 1735 (1971).
[6]R. H. Picard and C. R. Willis, Phys. Rev. A 8, 1536 (1973).
[7]R. Friedberg and S. R. Hartmann, Phys. Rev. A 10, 1728 (1974).
[8]C. T. Lee, Phys. Rev. A 13, 1657 (1976); 14, 1926 (1976).
[9]C. T. Lee, Phys. Rev. A 15, 2019 (1977); 16, 301 (1977).
[10]E. Ressayre and A. Tallet, Phys. Rev. A 15, 2410 (1977).
[11]A. Crubellier, Phys. Rev. A 15, 2430 (1977); A. Crubellier and M.-G. Schweighofer, *ibid.* 18, 1797 (1978).
[12]E. Ressayre and A. Tallet, Phys. Rev. A 18, 2196 (1978).
[12]R. J. Glauber and F. Haake, Phys. Lett. 68A, 29 (1978).
[14]F. Haake, H. King, G. Schroeder, J. Haus, R. Glauber, and F. Hopf, Phys. Rev. Lett. 42, 1740 (1979), and Phys. Rev. A 20, 2047 (1979).
[15]D. Polder, M. F. H. Schuurmans, and Q. H. F. Vrehen, Phys. Rev. A 19, 1192 (1979).
[16]R. Bonifacio, P. Schwendimann, and F. Haake, Phys. Rev. A 4, 302 (1971); 4, 854 (1971).
[17]L. M. Narducci, C. A. Coulter, and C. M. Bowden, Phys. Rev. A 9, 829 (1974).
[18]G. Banfi and R. Bonifacio, Phys. Rev. A 12, 2068 (1975).
[19]R. Bonifacio and L. A. Lugiato, Phys. Rev. A 11, 1507 (1975); 12, 587 (1975).
[20]R. Bonifacio, J. D. Farina, and L. M. Narducci, Opt. Commun. 31, 377 (1979).
[21]F. T. Arecchi and E. Courtens, Phys. Rev. A 2, 1730 (1970).
[22]C. R. Stroud, J. H. Eberly, W. L. Lama, and L. Mandel, Phys. Rev. A 5, 1094 (1972).
[23]R. Jodoin and L. Mandel, Phys. Rev. A 9, 873 (1974).
[24]J. C. MacGillivray and M. S. Feld, Phys. Rev. A 14, 1169 (1976).
[25]R. Saunders, S. S. Hassan, and R. K. Bullough, J. Phys. A 9, 1725 (1976).
[26]R. Saunders and R. K. Bullough, in Ref. 2, p. 209.
[27]F. A. Hopf and P. Meystre, Phys. Rev. A 12, 2534 (1975); F. A. Hopf, P. Meystre, and D. W. McLaughlin, *ibid.* 13, 777 (1976).
[28]R. Bonifacio, F. A. Hopf, P. Meystre, and M. O. Scully, Phys. Rev. A 12, 2568 (1975).
[29]J. A. Hermann, Phys. Lett. 67A, 253 (1978).
[30]J. A. Hermann, Opt. Commun. 28, 245 (1979).
[31]F. A. Hopf and E. A. Overman II, Phys. Rev. A 19, 1180 (1979); F. A. Hopf, *ibid.* 20, 2065 (1979).
[32]A. Icsevgi and W. E. Lamb, Phys. Rev. 185, 517 (1969).
[33]N. Skribanowitz, I. P. Herman, J. C. MacGillivray, and M. S. Feld, Phys. Rev. Lett. 30, 309 (1973).
[34]M. Gross, C. Fabre, P. Pillet, and S. Haroche, Phys. Rev. Lett. 36, 1035 (1976).
[35]A. Flusberg, T. Mossberg, and S. R. Hartmann, Phys. Lett. 58A, 373 (1976), and in Ref. 2, p. 37.
[36]Q. H. F. Vrehen, H. M. J. Hikspoors, and H. M. Gibbs, Phys. Rev. Lett. 38, 764 (1977); H. M. Gibbs, in Ref. 2, p. 61.
[37]H. M. Gibbs, Q. H. F. Vrehen, and H. M. J. Hikspoors, Phys. Rev. Lett. 39, 547 (1977); Q. H. F. Vrehen, in Ref. 2, p. 79; Q. H. F. Vrehen, H. M. J. Hikspoors, and H. M. Gibbs, in Ref. 3, p. 543.
[38]A. T. Rosenberger, S. J. Petuchowski, and T. A. DeTemple, in Ref. 2, p. 15, and in Ref. 3, p. 555.
[39]M. Gross, J. M. Raimond, and S. Haroche, Phys. Rev. Lett. 40, 1711 (1978).
[40]J. Okada, K. Ikeda, and M. Matsuoka, Opt. Commun. 26, 189 (1978); 27, 321 (1978).
[41]A. Crubellier, S. Liberman, and P. Pillet, Phys. Rev. Lett. 41, 1237 (1978).
[42]J. J. Ehrlich, C. M. Bowden, D. W. Howgate, S. H. Lehnigk, A. T. Rosenberger, and T. A. DeTemple, in Ref. 3, p. 923.
[43]Q. H. F. Vrehen and M. F. H. Schuurmans, Phys. Rev. Lett. 42, 224 (1979).
[44]F. Gounand, M. Hugon, P. R. Fournier, and J. Berlande, J. Phys. B 12, 547 (1979).
[45]M. Gross, P. Goy, C. Fabre, S. Haroche, and J. M. Raimond, Phys. Rev. Lett. 43, 343 (1979); J. Marek, J. Phys. B 12, L229 (1979); Ph. Cahuzac, H. Sontag, and P. E. Toschek, Opt. Commun. 31, 37 (1979).
[46]T. A. DeTemple, T. K. Plant, and P. D. Coleman, Appl. Phys. Lett. 22, 644 (1973).
[47]J. S. Murphy and J. E. Boggs, J. Chem. Phys. 47, 4152 (1967).
[48]W. K. Bischel, P. J. Kelly, and C. K. Rhodes, Phys. Rev. A 13, 1817 (1976).
[49]D. T. Hodges, J. R. Tucker, and T. S. Hartwick, Infrared Phys. 16, 175 (1976).
[50]T. A. DeTemple and E. J. Danielewicz, IEEE J. Quantum Electron. QE-12, 40 (1976).
[51]S. C. Wofsy, J. S. Muenter, and W. Klemperer, J. Chem. Phys. 55, 2014 (1971).
[52]S. M. Freund, G. Duxbury, M. Romheld, J. T. Tiedje, and T. Oka, J. Mol. Spectrosc. 52, 38 (1974).
[53]Z. Drozdowicz, R. J. Temkin, and B. Lax, IEEE J. Quantum Electron. QE-15, 170 (1979); QE-15, 865 (1979).
[54]See Ref. 52 and also E. Arimondo and M. Inguscio, J. Mol. Spectrosc. 75, 81 (1979).
[55]T. A. DeTemple and A. V. Nurmikko, Opt. Commun. 4, 321 (1971).
[56]E. Yablonovitch, Phys. Rev. A 10, 1888 (1974); H. S. Kwok and E. Yablonovitch, Appl. Phys. Lett. 27, 583 (1975).
[57]E. A. Jung and R. N. Lewis, Nucl. Instrum. Methods 44, 224 (1966).
[58]T. K. Plant and T. A. DeTemple, J. Appl. Phys. 47, 3042 (1976).
[59]P. Norton, J. Appl. Phys. 47, 308 (1976); Phys. Rev.

Lett. 37, 164 (1976). This detector has a response time between 2 and 10 nsec, depending on its bias voltage. The factor of 5 increase in speed at low bias, however, is accompanied by a decrease in sensitivity by a factor of about fifteen.

[60]To get absolute FIR intensity measurements, the Si:P detector response was calibrated using a chopped cw methyl fluoride waveguide laser as the source. The waveguide laser power was measured with a Scientech Model 3600 power meter, assuming an efficiency at 496 μm of 50%, as determined by Hodges *et al.*, Appl. Phys. Lett. 29, 662 (1976). Detector response was found as a function of bias voltage and chip resistance (temperature); these were monitored throughout the experiment. In use, FIR attenuators were used when necessary to ensure linear detector response.

[61]N is very nearly proportional to pressure p; as p increases, the fraction of the ground-state population excited by the pump increases slightly due to the contribution of homogeneous broadening to the off-resonant absorption. This adds a small nonlinear term. The fraction excited varies by less than 10% over the full range of pressures studied for any cell length.

[62]The average, rather than the maximum, is plotted because we feel that our pulses have not reached the steady state described in Refs. 27 and 28. The fluctuations observed are due to the means of excitation and are not true quantum fluctuations as discussed in Ref. 31.

[63]C. M. Bowden and C. C. Sung, Phys. Rev. A 18, 1558 (1978); 20, 2033 (1979). See also C. T. Lee, Phys. Rev. Lett. 43, 1110 (1979).

[64]A. Messiah, *Quantum Mechanics* (North-Holland, New York, 1959), p. 1072.

[65]These transitions differ in frequency from $K=2$ by 39 and 66 MHz (Table II). Beats in the observed FIR signal would appear at 39, 66, and 105 MHz were they not washed out by a combination of the large pulse bandwidth, amplifier and detector response, and transverse intensity variation.

[66]D. C. Burnham and R. Y. Chiao, Phys. Rev. 188, 667 (1969).

[67]In the course of our experiment, helium was introduced into the CH_3F cell in order to study the effect of enhanced collisional relaxation. The results pointed to a broadening rate substantially greater than that given for low-J CH_3F-He collisions in Ref. 48. This also makes us wary of extrapolating the self-broadening rate from low to high J.

[68]J.-C. Diels and E. L. Hahn, IEEE J. Quantum Electron. QE-12, 411 (1976).

[69]S. H. Lee, S. J. Petuchowski, A. T. Rosenberger and T. A. DeTemple, Opt. Lett. 4, 6 (1979); T. A. DeTemple, in *Proceedings of the International Conference on Lasers '78*, edited by V. Corcoran (STS Press, McLean, VA, 1979), pp. 104–110.

[70]W. Lemley and A. V. Nurmikko, Appl. Phys. Lett. 35, 33 (1979); W. Lemley, A. V. Nurmikko and B. J. Clifton, Int. J. Infrared Millimeter Waves 1, 85 (1980).

[71]H. K. Chung, A. T. Rosenberger, and T. A. DeTemple (unpublished).

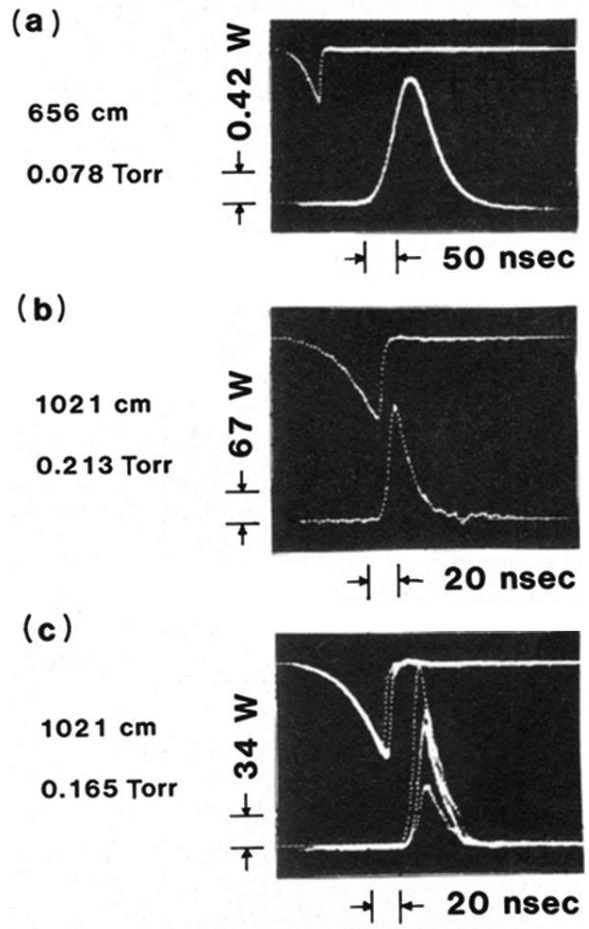

FIG. 3. Typical pulses, showing (a) superradiant pulse shape, with overshoot on trailing edge due to pulse amplifier; (b) a short superradaiant pulse without overshoot (amplifier was not used); (c) multiple exposure showing shot-to-shot fluctuation. In each case, the upper pulse is the truncated pump pulse and the vertical scale applies only to the FIR superradiant pulse.